THE JOURNAL OF PHYSICAL CHEMISTRY Letters

Letter

Cite This: J. Phys. Chem. Lett. 2017, 8, 5366-5371

pubs.acs.org/JPCL

# High Hole-Mobility Molecular Layer Made from Strong Electron Acceptor Molecules with Metal Adatoms

Hiroyuki Yamane*[,†,‡,§] and Nobuhiro Kosugi[†,‡]

[†]Institute for Molecular Science, National Institutes of Natural Sciences, Myodaiji, Okazaki 444-8585, Japan

[‡]SOKENDAI (The Graduate University for Advanced Studies), Myodaiji, Okazaki 444-8585, Japan

Supporting Information

**ABSTRACT:** The electronic structure of 7,7,8,8-tetracyanoquinodimethane (TCNQ) and 2,3,5,6-tetrafluoro-TCNQ ($F_4$TCNQ) monolayers on Au(111) has been investigated by means of angle-resolved photoemission spectroscopy (ARPES) with synchrotron radiation. In contrast to the physisorbed TCNQ/Au(111) interface, the high-resolution core-level photoemission spectra and the low-energy electron diffraction at the $F_4$TCNQ/Au(111) interface show evidence for the strong charge transfer (CT) from Au to $F_4$TCNQ and for the Au atom segregation from the underlying Au(111) surface, suggesting a possible origin of the spontaneous formation of the two-dimensional $F_4$TCNQ-Au network. The ARPES experiment reveals a low hole-injection barrier and large band dispersion in the CT-induced topmost valence level of the $F_4$TCNQ-Au network with 260 meV bandwidth due to the adatom-mediated intermolecular interaction. These results indicate that strong electron acceptor molecules with metal adatoms can form high hole-mobility molecular layers by controlling the molecule−metal ordered structure and their CT interaction.

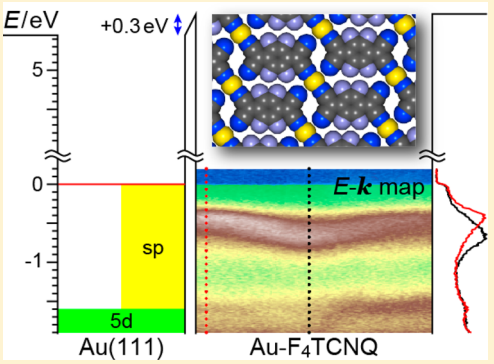


Two-dimensional (2D) atomic/molecular networks, e.g., graphene and supramolecular macrocyclic systems, and their layer-by-layer assemblies have attracted much attention for potential applications in (opto)electronics and energy storage because of their low-dimensional electron systems and nanoporous structures.[1−4] In order to fabricate functional molecular layers based on the selective assembly of the 2D network, the ordered structure of molecules, which dominates anisotropic physical and chemical properties, has to be designed by considering the molecular symmetry and the intermolecular interaction such as van der Waals, electrostatic, exchange, polarization, and charge-transfer (CT) interactions. Indeed, a large variety of molecular systems such as metal−organic frameworks (MOF) and covalent organic frameworks (COF) have been designed, and their 2D thin-film fabrications have been developed as a challenging issue.

Here, we shed light on the CT interaction in archetypical organic semiconductors. 7,7,8,8-Tetracyanoquinodimethane (TCNQ) and 2,3,5,6-tetrafluoro-TCNQ ($F_4$TCNQ) are well-known as electron acceptor molecules with large electron affinity and have been anticipated for the CT complex in combination with electron donor molecules,[5,6] for the p-type doping of molecules,[7−9] and for the control of the interfacial charge-injection barrier with respect to the highest occupied molecular orbital (HOMO) and/or the lowest unoccupied molecular orbital (LUMO).[10−15] The cyano group in TCNQ derivatives plays a crucial role in the strong electron-accepting ability in the CT interaction and often induces the *intra*- and/or *inter*-molecular structural relaxations such as the molecular distortion[16−18] and the 2D network formation,[19−22] depending on metal atoms and underlying surfaces; especially, the $F_4$TCNQ molecules on an Au(111) surface show both evidence for the strong molecular distortion and for the spontaneous formation of the 2D network via the cyano group with the Au adatom segregated from the underlying Au(111) surface as demonstrated using scanning tunneling microscopy (STM).[23,24]

Molecule−metal coordination systems have a large degree of freedom for the design of the 2D network structure and its functionalities. In order to understand characteristics of the 2D TCNQ-metal network systematically, we have studied the geometric and electronic structures of the $F_4$TCNQ/Au(111) and TCNQ/Au(111) interfaces as a benchmark by using low-energy electron diffraction (LEED) and angle-resolved photoemission spectroscopy (ARPES) with synchrotron radiation. We have succeeded in the observation of large in-plane band dispersion for the $F_4$TCNQ-derived electronic states, which are formed just below the Fermi level ($E_F$) by the strong CT from the Au atom to the $F_4$TCNQ molecule. The observed electronic interaction in the $F_4$TCNQ-Au network satisfies the high hole concentration ($n$) due to the low hole-injection barrier and also the high hole mobility ($\mu$) due to the large band dispersion in the conductivity formula $\sigma = ne\mu$.

**Received:** September 8, 2017
**Accepted:** October 18, 2017
**Published:** October 18, 2017





DOI: 10.1021/acs.jpclett.7b02390
J. Phys. Chem. Lett. 2017, 8, 5366−5371

As mentioned above, the cyano group in TCNQ derivatives plays a crucial role in the CT interaction. The strong CT interaction at the $F_4$TCNQ/Au(111) interface is clearly detected by the high-resolution N 1s photoemission spectra. As shown in Figure 1a, a neutral N 1s peak (labeled $N^0$)

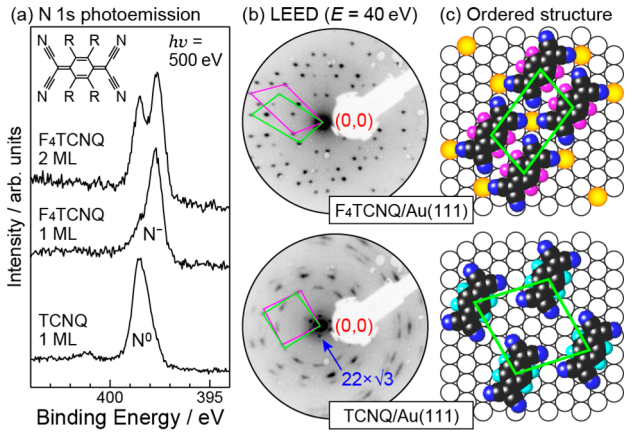


**Figure 1.** Chemical interaction and ordered structure at the $F_4$TCNQ/Au(111) and TCNQ/Au(111) interfaces at 20 K. (a) High-resolution N 1s photoemission spectra at 20 K obtained by $h\nu$ = 500 eV at the normal emission. The chemical structure of $F_4$TCNQ (R = F) and TCNQ (R = H) is given in the inset. (b) LEED image obtained by the electron energy of 40 eV. (c) Ordered structure in the real space determined from the LEED and previous STM data.[24,26] The segregated Au adatoms and the bulk-surface Au atoms are indicated by the yellow and white circles, respectively.

appears at the binding energy ($E_b$) of 398.5 eV for the 1 ML (monolayer) TCNQ on Au(111), indicating the physisorptive interaction at the TCNQ/Au(111) interface. On the other hand, the 1 ML $F_4$TCNQ on Au(111) shows a predominant N 1s peak at $E_b$ = 397.6 eV, which is lower than the $N^0$ peak in energy and is ascribed to the negatively charged N 1s (labeled $N^-$) due to the CT interaction at the interface. The $N^-$ peak is observable also for the 2 ML $F_4$TCNQ on Au(111) together with the $N^0$ peak, corresponding well with the concept of the extended space charge region for the $F_4$TCNQ multilayer on Au(111).[25] The strong CT interaction in general contributes to the ordered structure of the molecules. The LEED images in Figure 1b exhibit that the $F_4$TCNQ and TCNQ molecules on Au(111) form the different ordered structures to each other with the commensurate $\begin{pmatrix} 5 & 2 \\ 1 & 3 \end{pmatrix}$ structure for the $F_4$TCNQ/Au(111) interface and the incommensurate $\begin{pmatrix} 3.5 & -0.5 \\ 2.5 & 4.5 \end{pmatrix}$ structure for the TCNQ/Au(111) interface as shown in Figure 1c, as previously reported.[23−26] We found that the LEED image of the $F_4$TCNQ/Au(111) interface does not show the well-known $22 \times \sqrt{3}$ herringbone pattern of the Au(111) surface just around the (0,0) spot, which is clearly observable at the physisorbed TCNQ/Au(111) interface. Furthermore, we observed that the Au $4f_{7/2}$ photoemission line shape for the $F_4$TCNQ/Au(111) interface is slightly broader than that for the TCNQ/Au(111) interface because of the appearance of the new peak component at the low $E_b$ side (Figure S1 in the Supporting Information). The observed Au $4f_{7/2}$ photoemission line shape can be reproduced by considering the surface core-level shift due to the presence of bulk, surface, and adatom Au sites. These results support the validity of the present sample preparation in accordance with the earlier STM observation of the formation of the $F_4$TCNQ-Au network based on the Au-atom segregation from the Au(111) surface by the strong CT interaction between $F_4$TCNQ and Au.[24] As illustrated in Figure 1c, 1-$F_4$TCNQ molecule and 1-Au adatom exist in the oblique unit cell of the $F_4$TCNQ-Au network, where $F_4$TCNQ molecules are 2-fold coordinated with Au adatoms.

In addition to the ordered structure, the CT interaction introduces the significant change in the work function ($\Phi$) and the valence electronic structure. Figure 2a shows the normal-

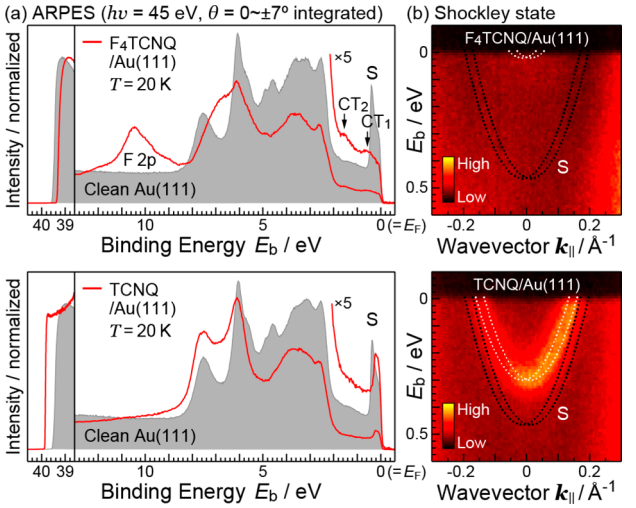


**Figure 2.** Electronic structure of the 1 ML films of $F_4$TCNQ and TCNQ on Au(111) at $T$ = 20 K. (a) Normal-emission ARPES spectra of the clean Au(111) surface (gray shadow) and the 1 ML films on Au(111) (red curve) measured using $h\nu$ = 45 eV. Left panel shows the secondary-electron cutoff. (b) $E$−$\mathbf{k}_{\parallel}$ map of the Shockley state. The white and black dashed lines represent the parabolic fitting to the observed dispersion for the 1 ML film and the clean Au(111) surface, respectively.

emission ARPES spectra [emission angle ($\theta$) of 0 ∼ ±7° integrated] measured for the $F_4$TCNQ/Au(111) and TCNQ/Au(111) interfaces. The secondary-electron cutoff for the TCNQ/Au(111) interface, shown in the left panel of Figure 2a, shifts to the higher $E_b$ side from that for the clean Au(111) surface. This higher-$E_b$ shift indicates the decrease in $\Phi$ upon the adsorption of TCNQ due to the Pauli repulsion (i.e., exchange interaction) of surface electrons at the interface ($\Delta\Phi$ = −0.34 eV). The opposite trend is observed for the $F_4$TCNQ/Au(111) interface, giving the shift in the secondary-electron cutoff to the lower $E_b$ side upon adsorption of $F_4$TCNQ, i.e., the increase in $\Phi$, due to CT from Au to $F_4$TCNQ ($\Delta\Phi$ = +0.27 eV), which overwhelms the contribution of the Pauli repulsion.

At the valence-band region for the $F_4$TCNQ/Au(111) interface (right panel of Figure 2a), the broad F 2p peak appears at $E_b$ = 10.4 eV, and the CT-induced valence peaks appear just below $E_F$; $E_b$ = 0.5 eV (labeled $CT_1$) and 1.5 eV (labeled $CT_2$), which can be ascribed to the filled LUMO due to CT and the former HOMO, respectively.[11,24] Furthermore, the Shockley-type surface state of Au(111) (labeled S) is almost quenched at the $F_4$TCNQ/Au(111) interface because of the significant electronic modification by $F_4$TCNQ as discussed later. On the other hand, the TCNQ-derived peak is not observable just below $E_F$, and the Shockley state is weakly modified with the shift to the lower $E_b$ side at the TCNQ/Au(111) interface. It has been understood that the modification


DOI: 10.1021/acs.jpclett.7b02390
J. Phys. Chem. Lett. 2017, 8, 5366−5371

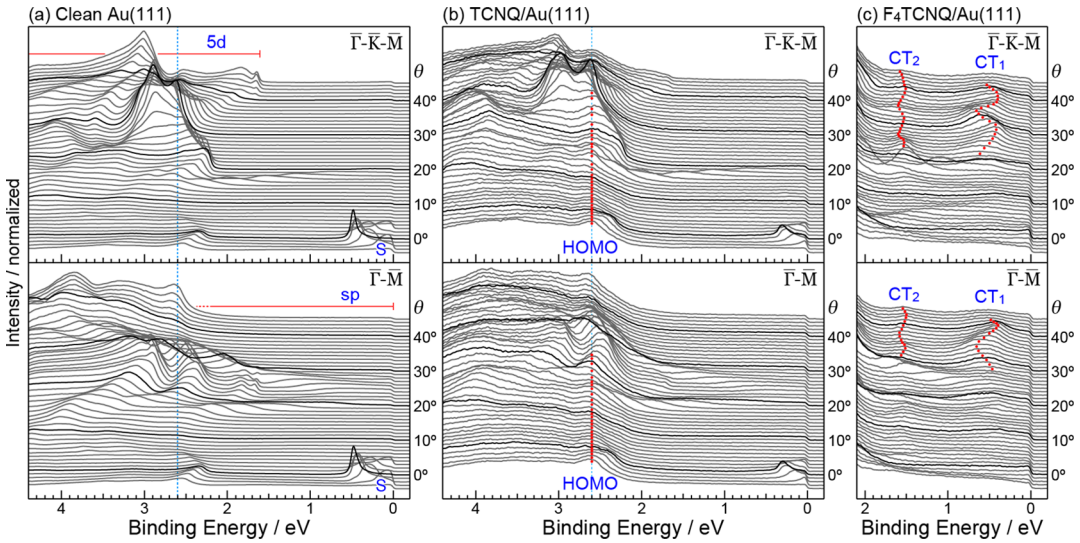


**Figure 3.** $\theta$-Dependent ARPES spectra along the $\bar{\Gamma}$-$\bar{K}$-$\bar{M}$ and $\bar{\Gamma}$-$\bar{M}$ directions at $T$ = 20 K: (a) clean Au(111) surface, (b) TCNQ monolayer on Au(111), and (c) $F_4$TCNQ monolayer on Au(111), shown with 1° step. The nondispersive HOMO-derived peak for TCNQ/Au(111) and the dispersive CT-derived peaks for $F_4$TCNQ/Au(111) are indicated by the red dots.

of the Shockley state by adsorbates is derived from the rearrangement of surface electron systems by complex interfacial interactions.[27−29] The lateral energy versus wavevector ($E$−$\mathbf{k}_{\|}$) map of the Shockley state is shown in Figure 2b as obtained using the relation of

$$\mathbf{k}_{\|} = [2m_0(h\nu - E_b - \Phi)]^{1/2}\sin\theta/\hbar$$

where $m_0$ is the free-electron mass. The Shockley state at the TCNQ/Au(111) interface shows a weak modification with the upshift by $\Delta E_b$ = 170 meV from that at the clean Au(111) surface, which is in general ascribed to the Pauli repulsion of surface electron systems. At the $F_4$TCNQ/Au(111) interface, the bottom tail of the Shockley state is barely observable at $E_b$ = 0 eV and $\mathbf{k}_{\|}$ = 0 Å$^{-1}$; in other words, the large upshift by more than 465 meV is induced as a result of the significant electronic modification due to the strong CT interaction at the interface. As demonstrated previously,[27,28] the observed shift in the Shockley state enables us to determine the interfacial adsorption energies, only 18.0 meV/Å$^2$ (= 0.106$\Delta E_b$) for the TCNQ/Au(111) interface, suggesting again the weak physisorptive interaction,[27] and more than 49.3 meV/Å$^2$ for the $F_4$TCNQ/Au(111) interface, which involves various interfacial electronic interactions.

In order to discuss the interfacial electronic interaction in more detail, the $\theta$-dependent ARPES spectra along the high-symmetry $\bar{\Gamma}$-$\bar{K}$-$\bar{M}$ and $\bar{\Gamma}$-$\bar{M}$ directions are shown in Figure 3. The clean Au(111) surface at 20 K shows the well-known electronic band dispersion for the Shockley state (S) around $\theta$ = 0°, sp band around $\theta$ = 20°, and 5d band in full-$\theta$ region. At the TCNQ/Au(111) interface at 20 K, the HOMO-derived peak is observable behind the Au 5d band at the constant $E_b$ position with $\theta$ ($E_b$ = 2.6 eV), and a quite weak signal from the deeper lying TCNQ-derived electronic state (HOMO−1) can be seen at $E_b$ = 4.0 eV at $\theta$ = 20−30°. The energy separation between HOMO and HOMO−1 by 1.4 eV corresponds well with the electronic structure of the TCNQ thick film.[30] The nondispersive HOMO and HOMO−1 peaks indicate the localized molecular electronic states at the TCNQ/Au(111) interface, while the CT-induced peaks ($CT_1$ and $CT_2$) at the $F_4$TCNQ/Au(111) interface at 20 K show a large dispersion with $\theta$, which is direct evidence for the delocalization of molecular electronic states. As shown in Figure 3c, the CT-induced peaks are getting visibly clearer at the higher $\theta$ ($\mathbf{k}_{\|}$) region, which is the reflection of the orbital-specific spatial electron distribution in ARPES.[22] The $CT_1$ peak appears at $E_b$ = 0.41 eV when $\theta$ = 27°. With increasing $\theta$, the $CT_1$ peak shifts to the higher $E_b$ side and turns back at around $\theta$ = 32°. The inflection point is also found at various $\theta$ such as 38°. Moreover, the dispersive behavior for the CT-induced peaks is observable not only at 20 K but also at 300 K (Figure S2).

The LEED analysis for the $F_4$TCNQ/Au interface using LEEDpat 4.2,[31] shown in Figure 4a, yields two domains of the $F_4$TCNQ-Au network structure that are rotated with respect to

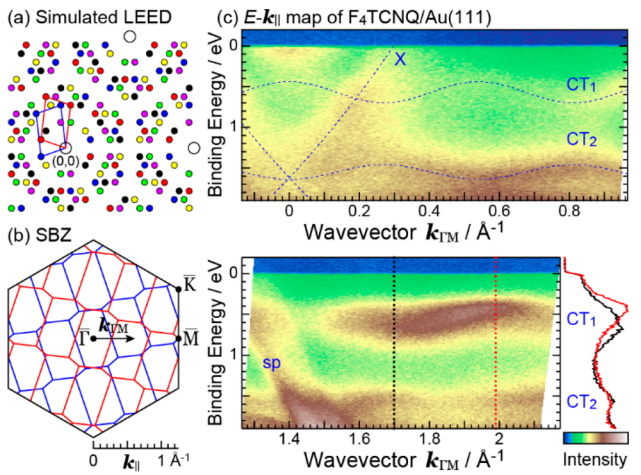


**Figure 4.** Valence-band dispersion at the $F_4$TCNQ/Au(111) interface. (a) Simulated LEED pattern, considering the (5, 2/1, 3) commensurate structure. The white and colored circles represent the diffraction spots from the substrate's and overlayer's lattices, respectively. (b) Surface Brillouin zone (SBZ) determined from the LEED pattern. The black and red/blue hexagons represent the substrate's SBZ and the example of the overlayer's SBZ, respectively. (c) Valence-band dispersion at 20 K obtained from the ARPES spectra along the $\bar{\Gamma}$-$\bar{M}$ direction. The eye-catching curves for the experimental dispersion are given as the blue dashed curve.



DOI: 10.1021/acs.jpclett.7b02390
J. Phys. Chem. Lett. 2017, 8, 5366−5371

the reciprocal unit cell of the 6-fold symmetric Au(111) surface. The multidomain overlayer structure introduces the intricate surface Brillouin zone (SBZ) as displayed in Figure 4b; therefore, it is in principle difficult to characterize the observed band dispersion for the multidomain films precisely. Remarkably, the $E-\mathbf{k}_{\parallel}$ map of the $F_4$TCNQ/Au(111) interface at 20 K along the high-symmetry $\bar{\Gamma}$-$\bar{M}$ direction ($\mathbf{k}_{\Gamma M}$), shown in Figure 4c, reveals the simple dispersion curves with a single component for the CT-induced states, probably due to the equivalent scanned region in two overlayer's SBZs as well as the matrix element effect in ARPES. Indeed, the $CT_1$ and $CT_2$ band dispersion curves get complex if the $E-\mathbf{k}_{\parallel}$ measurement is not performed along the high-symmetry directions (Figure S3).

The intensity of $CT_1$ is weaker than that of $CT_2$ at the low $\mathbf{k}_{\Gamma M}$ region (top panel of Figure 4c), and their relative intensity gets flipped at the higher $\mathbf{k}_{\Gamma M}$ region (bottom panel of Figure 4c), indicating different spatial electron distributions between the filled LUMO ($CT_1$) and the former HOMO ($CT_2$). From the line profile analysis for the $CT_1$-band dispersion at $\mathbf{k}_{\Gamma M}$ = 0−0.6 Å$^{-1}$, the dispersion center, bandwidth, and dispersion periodicity are determined as 0.57 ± 0.01 eV, 260 ± 10 meV, and 0.54 ± 0.02 Å$^{-1}$, respectively. The threshold $E_b$ position for the $CT_1$ band is determined to be 0.18 eV. The same dispersion periodicity is determined from the $CT_2$ band dispersion with the narrower bandwidth of 180 ± 10 meV. These dispersion curves give the first zone boundary at $\mathbf{k}_{\Gamma M}$ = 0.27 ± 0.02 Å$^{-1}$, in good agreement with the SBZ boundary determined from LEED as shown in Figure 4b; therefore, the observed dispersion can be ascribed to the $F_4$TCNQ-Au network structure and its electronic interaction.

The observed bandwidth for $CT_1$ by 260 ± 10 meV is comparable to the previously observed lateral band dispersions using ARPES for flat-lying organic monolayers on noble metal surfaces, which are categorized as the substrate-mediated band dispersion, e.g., 250 meV for pentacene on Cu(110),[32,33] 90 meV for iron and cobalt phthalocyanine (FePc and CoPc) on Au(110),[34] 230 meV for perylene-3,4,9,10-tetracarboxylic dianhydride (PTCDA) on Ag(110),[35] >500 meV for PTCDA on Cu(100),[36] 150 meV for naphthalene-1,4,5,8-tetracarboxylic dianhydride (NTCDA) on Ag(110),[37] and 200 meV for NTCDA on Cu(100).[37] The strong CT interaction between $F_4$TCNQ and Au could play a main role in the present large band dispersion and also introduce the decrease in the hole-injection barrier at the upper branch of the filled-LUMO band ($CT_1$). The free-electron-like parabolic fitting to the observed dispersion around the $\bar{\Gamma}$ point enables us to determine the hole effective mass ($m_h$*) as 0.46$m_0$ for $CT_1$ and 0.71$m_0$ for $CT_2$, both of which are heavier than that for Au sp band (0.27$m_0$) (Figure S4). According to the Bader analysis in the electron density distribution, 0.9 electrons contribute to the CT interaction in the $F_4$TCNQ-Au/Au(111) system and 0.29 and 0.61 electrons transfer from the Au(111) surface and the segregated Au adatom, respectively.[24] The heavier $m_h$* for $CT_1$ with respect to the Au sp band thus suggests that the observed dispersion mainly originates not from the "pure" substrate-mediated intermolecular interaction but from the adatom-mediated intermolecular interaction, which is invisible at the TCNQ/Au(111) interface. It was reported that a TCNQ-Mn network film on Ag(001), prepared by the vacuum deposition for both TCNQ and Mn, does not show the band dispersion for molecular electronic states, although the CT-derived peaks are formed just below $E_F$.[22] It was inferred that the lateral distance is too large in the ordered structure to mediate a significant lateral intermolecular interaction in the TCNQ-Mn network. The metal−atom segregation from the underlying substrate might be one of promising methods to fabricate functional molecule−metal coordination networks, where the electron affinity and the functional group in the molecule play a crucial role, as demonstrated in the present work. Considering the large degree of freedom for the design of the 2D network structure, the present observation for the delocalized CT band in the $F_4$TCNQ-Au/Au(111) system suggests possible realization of highly efficient molecular spintronic devices by choosing organic radicals or magnetic atoms in 2D molecule−metal hybrid networks, under adequate control of the network structure to delocalize molecular electronic states.

Finally, we briefly discuss the largely dispersive band at $\mathbf{k}_{\Gamma M}$ = 0∼ ± 0.3 Å$^{-1}$ (labeled X in Figure 4c), which is also observable in the raw ARPES spectra in Figure 3c as a quite weak signal at $\theta$ = 0−10°. If band X originates from a genuine molecular electronic state of the $F_4$TCNQ-Au network, it should appear with the same $\mathbf{k}_{\parallel}$ periodicity for the $CT_1$ and $CT_2$ bands. Because band X appears only around the $\bar{\Gamma}$ point, band X can be ascribed to the replica of the Au sp band due to the surface Umklapp scattering by the overlayer's lattice.[38] Further investigation using the low-$h\nu$ beam in ARPES is necessary for more confident assignment of band X.

In conclusion, the geometric and electronic structures of the $F_4$TCNQ-Au network, which is spontaneously formed at the $F_4$TCNQ/Au(111) interface, have been studied by means of LEED and ARPES with synchrotron radiation in comparison with the physisorbed TCNQ/Au(111) interface. The high-resolution core-level photoemission spectra and the LEED image of the $F_4$TCNQ/Au(111) interface comprehensively support the earlier finding of the $F_4$TCNQ-Au network formation,[24] originating from the Au atom segregation due to the CT interaction. Through the strong electron-accepting molecular functionality of $F_4$TCNQ, the CT interaction from Au to $F_4$TCNQ introduces the filling of LUMO, and the CT-induced electronic states are of temperature-independent delocalized character due to the stable adatom-mediated intermolecular interaction, as revealed from the ARPES experiments. The resultant filled-LUMO band has the characteristics of (i) the low hole-injection barrier by the threshold $E_b$ of 0.18 eV and (ii) the large bandwidth by 260 ± 10 meV with $m_h$* = 0.46$m_0$ at the $\bar{\Gamma}$ point, both of which satisfy the conductivity formula $\sigma = ne\mu$ as the high hole-mobility 2D molecular layer. All of the above characteristics are not observable at the TCNQ/Au(111) interface. The present finding can be a benchmark for the development of novel functional molecular materials based on molecule−metal coordination networks.

## EXPERIMENTAL METHODS

The present ARPES experiment was performed on a highly brilliant in-vacuum undulator beamline BL6U of the UVSOR-III Synchrotron in the Institute for Molecular Science (Okazaki, Japan). The BL6U covers the photon energy from 40 to 800 eV with a photon flux of ca. $10^{11}$ photons/sec under the top-up operation. The ARPES endstation at BL6U consists of the measurement, preparation, and load-lock chambers in UHV.

The clean Au(111) substrate was obtained by repeated cycles of $Ar^+$ sputtering and the subsequent annealing at 700 K, as confirmed by LEED with a microchannel-plate (MCP) detector and by the Shockley state in ARPES. In order to obtain the ordered monolayers of $F_4$TCNQ and TCNQ on Au(111), the



DOI: 10.1021/acs.jpclett.7b02390
J. Phys. Chem. Lett. 2017, 8, 5366−5371

thin multilayer sample with the layer thickness of ca. 50 Å was heated at above the multilayer desorption temperature of 380 K, which is slightly lower than the desorption temperature of the $F_4$TCNQ and TCNQ monolayers on Au(111), as confirmed by ARPES (Figure S5). The lateral ordered structure of organic layers was confirmed by MCP-LEED.

The ARPES spectra were acquired from the energy versus angle image by using the MCP detector of a hemispherical electron energy analyzer (MB Scientific A-1). All ARPES spectra shown in this Letter were measured at 20 K by using the liquid He cryostat (Janis ST400-UHV) in the six-axes ($x$, $y$, $z$, polar, and azimuth) manipulator. For the secondary-electron-cutoff (i.e., work function) measurement in ARPES, the negative bias of −5.000 V was applied to the sample to observe photoelectrons close to the zero-kinetic energy. The $E_b$ position for the valence-band and core-level ARPES spectra was calibrated by measuring the $E_F$ edge and the Au 4f peak of the underlying Au(111) substrate, respectively.

## ■ ASSOCIATED CONTENT

### Supporting Information

The Supporting Information is available free of charge on the ACS Publications website at DOI: 10.1021/acs.jpclett.7b02390.

Extra experimental data and corresponding discussion; high-resolution Au $4f_{7/2}$ photoemission spectra, temperature dependence of ARPES, azimuthal-angle dependence of the CT-band dispersion, fitting analysis of the CT-band dispersion, and annealing-temperature dependence of ARPES (PDF)

## ■ AUTHOR INFORMATION


### Corresponding Author

*E-mail: yamane@spring8.or.jp.

### ORCID

Hiroyuki Yamane: 0000-0002-8023-7918

### Present Address

§H.Y.: RIKEN Spring-8 Center, Sayo, Hyogo 679−5148, Japan.


### Notes

The authors declare no competing financial interest.

## ■ ACKNOWLEDGMENTS

The authors thank the staff of the UVSOR-III Synchrotron for their kind support in the present ARPES experiment. This work is supported by Grant-in-Aid for Scientific Research on Innovative Areas ($\pi$-System Figuration: Control of Electron and Structural Dynamism for Innovative Functions) JP17H05167 and Grant-in-Aid for Scientific Research (C) JP17K05767 from Japan Society for the Promotion of Science (JSPS) and Grant for Basic Science Research Projects from the Sumitomo Foundation 150301.

## ■ REFERENCES


(1) Barth, J. V.; Costantini, G.; Kern, K. Engineering Atomic and Molecular Nanostructures at Surfaces. *Nature* **2005**, *437*, 671−679.

(2) Jariwala, D.; Marks, T. J.; Hersam, M. C. Mixed-Dimensional van der Waals Heterostructures. *Nat. Mater.* **2017**, *16*, 170−181.

(3) Trickett, C. A.; Helal, A.; Al-Maythalony, B. A.; Yamani, Z. H.; Cordova, K. E.; Yaghi, O. M. The Chemistry of Metal-Organic Frameworks for $CO_2$ Capture, Regeneration and Conversion. *Nat. Rev. Mater.* **2017**, *2*, 17045.

(4) Huang, N.; Wang, P.; Jiang, D. Covalent Organic Frameworks: A Materials Platform for Structural and Functional Designs. *Nat. Rev. Mater.* **2016**, *1*, 16068.

(5) Ferraris, J.; Cowan, D. O.; Walatka, V.; Perlstein, J. H. Electron Transfer in a New Highly Conducting Donor-Acceptor Complex. *J. Am. Chem. Soc.* **1973**, *95*, 948−949.

(6) Claessen, R.; Sing, M.; Schwingenschlögl, U.; Blaha, P.; Dressel, M.; Jacobsen, C. S. Spectroscopic Signatures of Spin-Charge Separation in the Quasi-One-Dimensional Organic Conductor TTF-TCNQ. *Phys. Rev. Lett.* **2002**, *88*, 096402.

(7) Gao, W.; Kahn, A. Controlled P-Doping of Zinc Phthalocyanine by Coevaporation with Tetrafluorotetracyanoquinodimethane: A Direct and Inverse Photoemission Study. *Appl. Phys. Lett.* **2001**, *79*, 4040−4042.

(8) Gao, W.; Kahn, A. Electronic Structure and Current Injection in Zinc Phthalocyanine Doped with Tetrafluorotetracyanoquinodimethane: Interface Versus Bulk Effects. *Org. Electron.* **2002**, *3*, 53−63.

(9) Gao, W.; Kahn, A. Controlled P Doping of the Hole-Transport Molecular Material N,N′-diphenyl-N,N′-bis(1-naphthyl)-1,1′-biphenyl-4,4′-diamineN,N′-diphenyl-N,N′-bis(1-naphthyl)-1,1′-biphenyl-4,4′-diamine with Tetrafluorotetracyanoquinodimethane. *J. Appl. Phys.* **2003**, *94*, 359−366.

(10) Koch, N.; Duhm, S.; Rabe, J. P.; Vollmer, A.; Johnson, R. L. Optimized Hole Injection with Strong Electron Acceptors at Organic-Metal Interfaces. *Phys. Rev. Lett.* **2005**, *95*, 237601.

(11) Romaner, L.; Heimel, G.; Brédas, J.-L.; Gerlach, A.; Schreiber, F.; Johnson, R. L.; Zegenhagen, J.; Duhm, S.; Koch, N.; Zojer, E. Impact of Bidirectional Charge Transfer and Molecular Distortions on the Electronic Structure of a Metal-Organic Interface. *Phys. Rev. Lett.* **2007**, *99*, 256801.

(12) Qi, D.; Chen, W.; Gao, X.; Wang, L.; Chen, S.; Loh, K. P.; Wee, A. T. S. Surface Transfer Doping of Diamond (100) by Tetrafluorotetracyanoquinodimethane. *J. Am. Chem. Soc.* **2007**, *129*, 8084−8085.

(13) Rangger, G. M.; Hofmann, O. T.; Romaner, L.; Heimel, G.; Bröker, B.; Blum, R.-P.; Johnson, R. L.; Koch, N.; Zojer, E. F4TCNQ on Cu, Ag, and Au as Prototypical Example for a Strong Organic Acceptor on Coinage Metals. *Phys. Rev. B: Condens. Matter Mater. Phys.* **2009**, *79*, 165306.

(14) Coletti, C.; Riedl, C.; Lee, D. S.; Krauss, B.; Patthey, L.; von Klitzing, K.; Smet, J. H.; Starke, U. Charge Neutrality and Band-Gap Tuning of Epitaxial Graphene on SiC by Molecular Doping. *Phys. Rev. B: Condens. Matter Mater. Phys.* **2010**, *81*, 235401.

(15) Yoshimoto, S.; Kameshima, K.; Koitaya, T.; Harada, Y.; Mukai, K.; Yoshinobu, J. Interface State and Energy Level Alignment of F4-TCNQ Sandwiched Between a Pentacene Film and the Ethylene-Terminated Si(100) Surface. *Org. Electron.* **2014**, *15*, 356−364.

(16) Romaner, L.; Heimel, G.; Brédas, J.-L.; Gerlach, A.; Schreiber, F.; Johnson, R. L.; Zegenhagen, J.; Duhm, S.; Koch, N.; Zojer, E. Impact of Bidirectional Charge Transfer and Molecular Distortions on the Electronic Structure of a Metal-Organic Interface. *Phys. Rev. Lett.* **2007**, *99*, 256801.

(17) Katayama, T.; Mukai, K.; Yoshimoto, S.; Yoshinobu, J. Thermally Activated Transformation from a Charge-Transfer State to a Rehybridized State of Tetrafluoro-tetracyanoquinodimethane on Cu(100). *J. Phys. Chem. Lett.* **2010**, *1*, 2917−2921.

(18) Kumar, A.; Banerjee, K.; Dvorak, M.; Schulz, F.; Harju, A.; Rinke, P.; Liljeroth, P. Charge-Transfer-Driven Nonplanar Adsorption of $F_4$TCNQ Molecules on Epitaxial Graphene. *ACS Nano* **2017**, *11*, 4960−4968.

(19) Shi, X. Q.; Lin, C.; Minot, C.; Tseng, T.-C.; Tait, S. L.; Lin, N.; Zhang, R. Q.; Kern, K.; Cerdá, J. I.; Van Hove, M. A. Structural Analysis and Electronic Properties of Negatively Charged TCNQ: 2D Networks of $(TCNQ)_2Mn$ Assembled on Cu(100). *J. Phys. Chem. C* **2010**, *114*, 17197−17204.

(20) Tseng, T.-C.; Abdurakhmanova, N.; Stepanow, S.; Kern, K. Hierarchical Assembly and Reticulation of Two-Dimensional Mn- and Ni-$TCNQ_x$ ($x$ = 1, 2, 4) Coordination Structures on a Metal Surface. *J. Phys. Chem. C* **2011**, *115*, 10211−10217.




DOI: 10.1021/acs.jpclett.7b02390
J. Phys. Chem. Lett. 2017, 8, 5366−5371

(21) Abdurakhmanova, N.; Tseng, T.-C.; Langner, A.; Kley, C. S.; Sessi, V.; Stepanow, S.; Kern, K. Superexchange-Mediated Ferromagnetic Coupling in Two-Dimensional Ni-TCNQ Networks on Metal Surfaces. *Phys. Rev. Lett.* **2013**, *110*, 027202.
(22) Feyer, V.; Graus, M.; Nigge, P.; Zamborlini, G.; Acres, R. G.; Schöll, A.; Reinert, F.; Schneider, C. M. The Geometric and Electronic Structure of TCNQ and TCNQ+Mn on Ag(001) and Cu(001) Surfaces. *J. Electron Spectrosc. Relat. Phenom.* **2015**, *204*, 125−131.
(23) Jäckel, F.; Perera, U. G. E.; Iancu, V.; Braun, K.-F.; Koch, N.; Rabe, J. P.; Hla, S.-W. Investigating Molecular Charge Transfer Complexes with a Low Temperature Scanning Tunneling Microscope. *Phys. Rev. Lett.* **2008**, *100*, 126102.
(24) Faraggi, M. N.; Jiang, N.; Gonzalez-Lakunza, N.; Langner, A.; Stepanow, S.; Kern, K.; Arnau, A. Bonding and Charge Transfer in Metal-Organic Coordination Networks on Au(111) with Strong Acceptor Molecules. *J. Phys. Chem. C* **2012**, *116*, 24558−24565.
(25) Gerbert, D.; Maass, F.; Tegeder, P. Extended Space Charge Region and Unoccupied Molecular Band Formation in Epitaxial Tetrafluoro-Tetracyanoquinodimethane Films. *J. Phys. Chem. C* **2017**, *121*, 15696−15701.
(26) Fernández-Torrente, I.; Franke, K. J.; Pascual, J. I. Structure and Electronic Configuration of Tetracyanoquinodimethane Layers on a Au(111) Surface. *Int. J. Mass Spectrom.* **2008**, *277*, 269−273.
(27) Ziroff, J.; Gold, P.; Bendounan, A.; Forster, F.; Reinert, F. Adsorption Energy and Geometry of Physisorbed Organic Molecules on Au(111) Probed by Surface-State Photoemission. *Surf. Sci.* **2009**, *603*, 354−358.
(28) Yamane, H.; Kosugi, N. Site-Specific Organic/Metal Interaction Revealed from Shockley-Type Interface State. *J. Phys. Chem. C* **2016**, *120*, 24307−24313.
(29) Armbrust, N.; Schiller, F.; Güdde, J.; Höfer, U. Model Potential for the Description of Metal/Organic Interface States. *Sci. Rep.* **2017**, *7*, 46561.
(30) Capitán, M. J.; Navío, C.; Beltrán, J. I.; Otero, R.; Álvarez, J. TCNQ Grown on Cu(001): Its Atomic and Electronic Structure Determination. *J. Phys. Chem. C* **2016**, *120*, 26889−26898.
(31) Hermann, K. E.; Van Hove, M. A. *LEEDpat*, version 4.2; 2014; see also http://www.fhi-berlin.mpg.de/KHsoftware/LEEDpat/index.html.
(32) Yamane, H.; Yoshimura, D.; Kawabe, E.; Sumii, R.; Kanai, K.; Ouchi, Y.; Ueno, N.; Seki, K. Electronic Structure at Highly Ordered Organic/Metal Interfaces: Pentacene on Cu(110). *Phys. Rev. B: Condens. Matter Mater. Phys.* **2007**, *76*, 165436.
(33) Ules, T.; Lüftner, D.; Reinisch, E. M.; Koller, G.; Puschnig, P.; Ramsey, M. G. Orbital Tomography of Hybridized and Dispersing Molecular Overlayers. *Phys. Rev. B: Condens. Matter Mater. Phys.* **2014**, *90*, 155430.
(34) Betti, M. G.; Gargiani, P.; Frisenda, R.; Biagi, R.; Cossaro, A.; Verdini, A.; Floreano, L.; Mariani, C. Localized and Dispersive Electronic States at Ordered FePc and CoPc Chains on Au(110). *J. Phys. Chem. C* **2010**, *114*, 21638−21644.
(35) Wießner, M.; Ziroff, J.; Forster, F.; Arita, M.; Shimada, K.; Puschnig, P.; Schöll, A.; Reinert, F. Substrate-Mediated Band-Dispersion of Adsorbate Molecular States. *Nat. Commun.* **2013**, *4*, 1514.
(36) Lüftner, D.; Hurdax, P.; Koller, G.; Puschnig, P.; Ramsey, M. G.; Weiß, S.; Yang, X.; Soubatch, S.; Tautz, F. S.; Feyer, V.; Gottwald, A. Understanding the Photoemission Distribution of Strongly Interacting Two-Dimensional Overlayers. *Phys. Rev. B: Condens. Matter Mater. Phys.* **2017**, *96*, 125402.
(37) Wießner, M.; Kübert, J.; Feyer, V.; Puschnig, P.; Schöll, A.; Reinert, F. Lateral Band Formation and Hybridization in Molecular Monolayers: NTCDA on Ag(110) and Cu(100). *Phys. Rev. B: Condens. Matter Mater. Phys.* **2013**, *88*, 075437.
(38) Bocquet, F. C.; Giovanelli, L.; Amsalem, P.; Petaccia, L.; Topwal, D.; Gorovikov, S.; Abel, M.; Koch, N.; Porte, L.; Goldoni, A.; et al. Final-State Diffraction Effects in Angle-Resolved Photoemission at an Organic-Metal Interface. *Phys. Rev. B: Condens. Matter Mater. Phys.* **2011**, *84*, 241407.



DOI: 10.1021/acs.jpclett.7b02390
*J. Phys. Chem. Lett.* 2017, 8, 5366−5371